ADVANCED FUNCTIONAL MATERIALS
www.afm-journal.de

Valence-Optimized Vanadium Oxide Supercapacitor Electrodes Exhibit Ultrahigh Capacitance and Super-Long Cyclic Durability of 100 000 Cycles

Minghao Yu, Yan Zeng, Yi Han, Xinyu Cheng, Wenxia Zhao, Chaolun Liang, Yexiang Tong, Haolin Tang, and Xihong Lu**

Vanadium oxides (VO_x) have been intensely investigated as cathode materials for SCs due to the multiple stable oxidation states (III–V) of vanadium in its oxides and typical layered structure. Nevertheless, fast capacity fading is always observed for VO_x upon cycling in aqueous electrolyte. Developing an efficient strategy to essentially promote the durability of VO_x in mild aqueous electrolyte remains a crucial challenge. Here, an innovative and effective method is reported to significantly boost the durability and capacitance of VO_x through tuning the valence state of vanadium. The valence state of vanadium is optimized through a very facile electrochemical oxidation method. A superior electrochemical performance and an ultralong cyclic stability of 100 000 cycles are obtained for these electrodes. An in-depth study on the variation for the valence state of vanadium during the oxidation process and the cyclic stability test indicates that the long cyclic stability has an important relationship with the distribution of the valence state of vanadium.

1. Introduction

Owning to the ever-worsening environmental deterioration and energy depletion, rechargeable energy storage technology has evoked wide interests in recent years.[1] Supercapacitors (SCs), also called electrochemical capacitors, are emerging as the most promising energy storage devices for the future due to their specific advantages of fast power release and long-term stability over other storage devices.[2] Aimed at their low energy density, the main research has been focused on developing alternative pseudo-capacitive electrode materials to replace the commercialized carbon electrode, which has the bad traits of low specific capacitance. In particular, vanadium oxides (VO_x), which are earth-abundant and inexpensive, have been intensely investigated as cathode materials for SCs.[3] The multiple stable oxidation states (III–V) of vanadium in its oxides and typical layered structures enable VO_x to have an even higher charge storage capability than most of other inexpensive transition-metal oxides. Unfortunately, early studies[3a,e] identified that fast capacity fading is always being observed for VO_x upon cycling in aqueous electrolyte, which is associated with the formation of soluble species ($H_2VO_4^-$ or HVO_4^{2-}) and structural degradation induced by repeated ion intercalation/deintercalation. For instance, Perera et al.[3d] reported a kind of SC based on VO_x nanowire cathodes, which exhibited a large capacitance loss of almost 40% after only 100 cycles. Such poor cycling stability definitely failed the target of long-term cycling performance as expected for supercapacitor applications (>10 000 cycles). Several attempts have been tried to address this limitation, like coating a thin inert layer to strengthen their mechanical stability,[3l,4] and replacing aqueous electrolyte with organic or quasi-solid-state electrolyte to relieve their dissolution.[3j,5] Most recently, a huge breakthrough was realized by Wang et al.,[3j] who designed a kind of gel polymer electrolyte with less water content based on polyving akohol and LiCl. This gel polymer electrolyte could efficiently avoid structural collapse and prevent chemical dissolution, resulting in a remarkable stability of up to 5000 cycles with only 15% capacity loss. Nevertheless, both inert protection layer and gel polymer electrolytes would more or less lengthen the ion pathway and enlarge the inner impedance. Developing an efficient strategy to essentially promote the durability of VO_x in mild aqueous electrolyte remains a scientific and technical challenge.

The valence state of V has been reported to play a key role in the electronic and electrochemical performance of VO_x electrodes.[6] We anticipated that tuning the proportion of different valence states of V could optimize the reversible reaction

M. Yu, Y. Zeng, Prof. H. Tang
State Key Laboratory of Advanced Technology for Materials Synthesis and Processing
Wuhan University of Technology
Wuhan 430070, P. R. China
E-mail: thln@whut.edu.cn
M. Yu, Y. Han, X. Cheng, Prof. Y. Tong, Prof. X. Lu
MOE of the Key Laboratory of Bioinorganic and Synthetic Chemistry
KLGHEI of Environment and Energy Chemistry
School of Chemistry and Chemical Engineering
Sun Yat-Sen University
Guangzhou 510275, P. R. China
E-mail: luxh6@mail.sysu.edu.cn
Dr. W. X. Zhao, C. L. Liang
Instrumental Analysis and Research Center
Sun Yat-Sen University
Guangzhou 510275, P. R. China

DOI: 10.1002/adfm.201501342

in VO_x electrodes during the charging/discharging process, hence enhancing its capacitance as well as cyclic stability. In this work, we reported an innovative and powerful strategy to achieve long cycling life and enhanced capacitance of VO_x SC electrodes by tuning the valence state of V. Porous VO_x electrode with excellent electrochemical performances was obtained by a facile electrochemical oxidation of V_2O_3 with a low voltage of 0.7 V for only 20 s. The presented method has significant advantages of simpleness, energy- and time-saving, and low cost, hence holding great promise to be macroscopically realized in industrial production. The as-prepared VO_x electrode not only reached a large areal capacitance of 356.8 mF cm^{-2} (corresponding gravimetric capacitance of 637.1 F g^{-1}) at 0.5 mA cm^{-2}, but also exhibited an abnormal long-term cycling stability without any decay of capacitance after 100 000 cycles. In-depth investigations revealed that only slight dissolution of VO_x into electrolyte occurred, and the finally VO_x electrode was stabilized with a proper proportion of V^{3+}, V^{4+}, and V^{5+}, which enables reversible conversion between them during the charge–discharge processes. Moreover, the already dissolved V in electrolyte also efficiently limited the further dissolve of active material in electrode.

2. Results and Discussion

2.1. Optimization of V Valence State in VO_x

The newly designed strategy for promoting VO_x long durability avoids the use of complex steps, and long reaction time. Herein, V_2O_3 nanorods were first synthesized on carbon cloth substrate as precursor through a combinative method of hydrothermal and annealing in hydrogen (Experimental Section). Scanning electron microscopy (SEM) images (**Figure 1**a) reveal that the as-prepared nanorods uniformly cover the surface of carbon fabric. Each nanorod has a diameter of 80–150 nm and length of about 500 nm. Then, the facile electro-oxidation process was conducted to a piece of V_2O_3 electrode using a low voltage of only 0.7 V in a three-electrode cell with 5 M LiCl aqueous electrolyte for 20 s. A Pt wire was used as a counter electrode, while a saturated calomel electrode (SCE) was used as a reference electrode. Figure 1b highlights the overall morphology after electro-oxidation (denoted as VO_x). The originally vertical rod fell down and spontaneously formed an interconnected network tangled the whole carbon fabric with numerous macro pores scattered. Meanwhile, a color change, turning to light yellow, was also observed for the colorless LiCl electrolyte, which indicates the formation of soluble species containing V element (Figure S1, Supporting Information). The mass loading of VO_x dramatically decreased into 0.56 mg cm^{-2}, while the mass loading of V_2O_3 was 1.48 mg cm^{-2}. All these signs verified the morphology evolution and partial dissolution during the oxidation process. Figure 1c presents the X-ray diffraction (XRD) pattern of VO_x in comparison with V_2O_3. The diffraction peaks of original V_2O_3 can be well indexed as rhombohedral V_2O_3 (JCPDS no. 65-9474). After the oxidation, only a broad peak at 26.6° corresponding to the (004) plane of carbon fabric was remained, suggesting the amorphous state of the new-formed VO_x. The microstructure variation during the oxidation process was further characterized by transmission electron microscopy (TEM). Typical TEM images of a V_2O_3 nanorod are demonstrated in Figure 1d. The single crystal structure is confirmed by its selected area electron diffraction (SAED) pattern (Figure 1e). An interplanar spacing of 0.37 nm is shown in high-resolution TEM images (Figure 1f), which coincides with the (012) facets of rhombohedral V_2O_3. In contrast, a much looser structure with rod shape collapsed was detected for VO_x in its TEM image. The highly diffusive ring pattern (inset) in the SAED pattern verifies the amorphous structure of VO_x, which is consistent with XRD information. Furthermore, electron energy loss spectroscopy (EELS) spectra

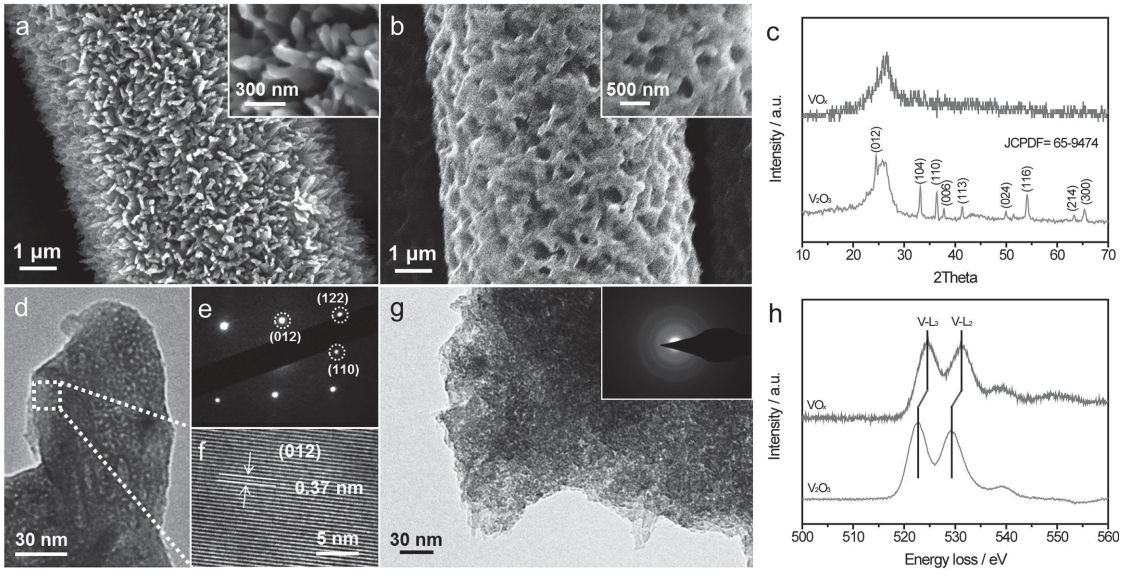

Figure 1. SEM images of as-prepared a) V_2O_3 and b) VO_x samples. c) XRD spectra collected for as-prepared V_2O_3 and VO_x samples. d) TEM image, e) SAED pattern, and f) HRTEM images of a V_2O_3 nanorod. g) TEM image and corresponding SAED pattern of a VO_x sample. h) EELS spectra collected for as-prepared V_2O_3 and VO_x samples.

were measured to preliminarily evaluate the valence state of V element (Figure 1h). Both spectra of V L-edge consist of two typical peaks named as L_2 (corresponding to two $2p^{1/2} \rightarrow 3d^{3/2}$) and L_3 (corresponding to four $2p^{3/2} \rightarrow 3d^{3/2}3d^{5/2}$). From the right-shift position of the L_2 and L_3 peak maximum, it is easy to determine that the valence of V changed from V^{3+} to V^{4+} and V^{5+}.[7] Therefore, the V_2O_3 was successfully oxidized to a higher valance state.

2.2. Study on the Variation of V Valence State

In order to highlight the possible phase and composition change inside VO_x during the oxidation process, electron paramagnetic resonance (EPR) and Raman spectra were characterized for V_2O_3 and VO_x samples. **Figure 2**a displays the EPR spectra of pristine V_2O_3 and VO_x samples. It is clearly shown that no significant peak was obtained for the V_2O_3 sample due to completely paired electrons in V (+3). In contrast, a certain amount of V (+4) was detected in the VO_x sample, as evidenced by its characteristic eight-line spectrum produced by the coupling of the unpaired electron of the vanadium (IV) with the spin = 7/2 vanadium nucleus.[8] Notably, the existence of V (+5) cannot be determined by EPR results due to its completely paired electrons. However, the newly formed Raman peaks for the VO_x sample (Figure 2b) match well with VO_2 and V_2O_5, respectively,[9] indicating that our VO_x samples contained not only V (+4) but also V (+5). Since EPR and Raman spectra provide the bulk composition information of VO_x samples, X-ray photoelectron spectroscopy (XPS) analyses, only detecting the electrode with a few nanometers depth, were further performed to assess the surface compositions of the samples. The XPS survey spectra indicate that both V_2O_3 and VO_x contain only C, V, and O without other detectable impurities on their surfaces (Figure 2c). Particularly, a comparison provides an understanding of surface V. Figure 2d compares the high-resolution V 2p 3/2 XPS spectra of the V_2O_3 and VO_x samples. Both V 2p 3/2 signals are deconvoluted into three peaks located at 515.9, 516.5, and 517.5 eV, which can be attributed to the signals for V^{3+}, V^{4+}, and V^{5+}.[6b,10] The existence of V^{4+} and V^{5+} in V_2O_3 sample is due to the inevitable oxidation of surface V_2O_3 when it is exposed to air. Interestingly, after the oxidation of V_2O_3, the relative proportion of V^{4+} decreased from 19.4 to 10.7%, accompanied with the increase of V^{5+} from 67.8 to 76.0%, while only slight change was obtained for V^{3+} (from 12.8 to 13.3%). As reported in previous literatures, this enriched V^{5+} is hoped to bring more capacitive activity to our VO_x sample.[3c,k,6a]

2.3. Electrochemical Performance of VO_x Electrode

Next, we evaluated the electrochemical performance of VO_x with V valence state tuned using the previous three-electrode cell by means of cyclic voltammetry (CV), galvanostatic charge–discharge, and electrochemical impedance spectroscopy (EIS). To optimize the proportion of V^{3+}, V^{4+}, and V^{5+}, thereby realizing the best electrochemical performance, the electrochemical oxidization time was firstly studied. A short time of 20 s was selected as the optimal time taking their XPS results (Figure S2, Supporting Information) and CV curves (Figure S3, Supporting

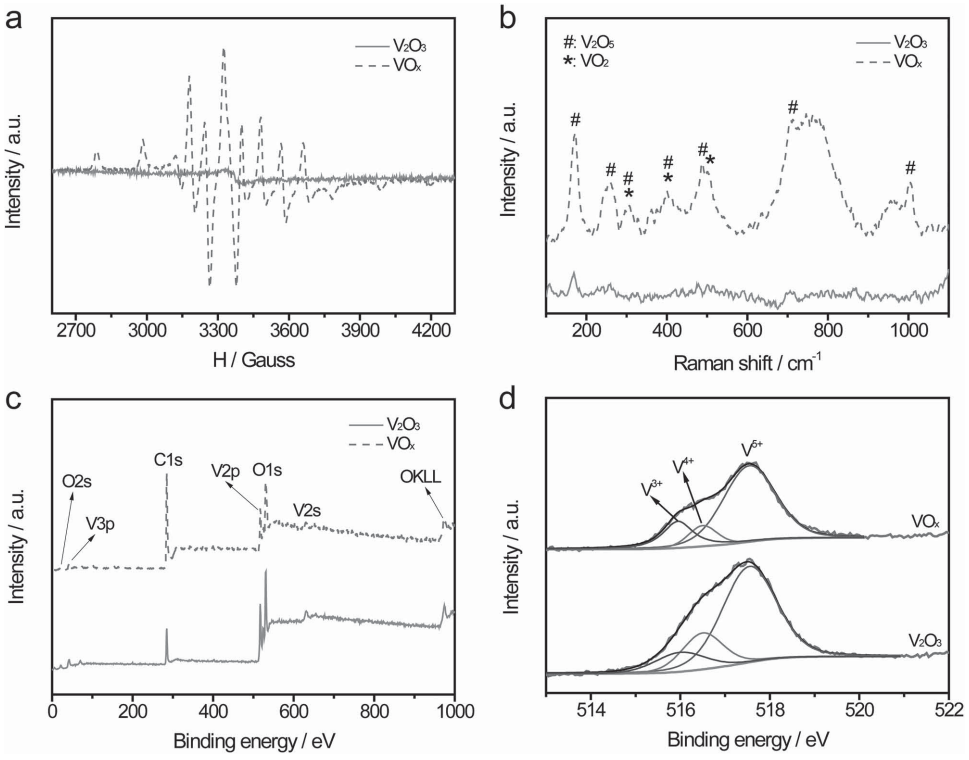

Figure 2. a) EPR spectra, b) Raman spectra, c) survey XPS spectra, and d) V 2p 3/2 XPS spectra of V_2O_3 and VO_x samples. The EPR spectra were collected at 100 K, where *H* is the magnetic field.

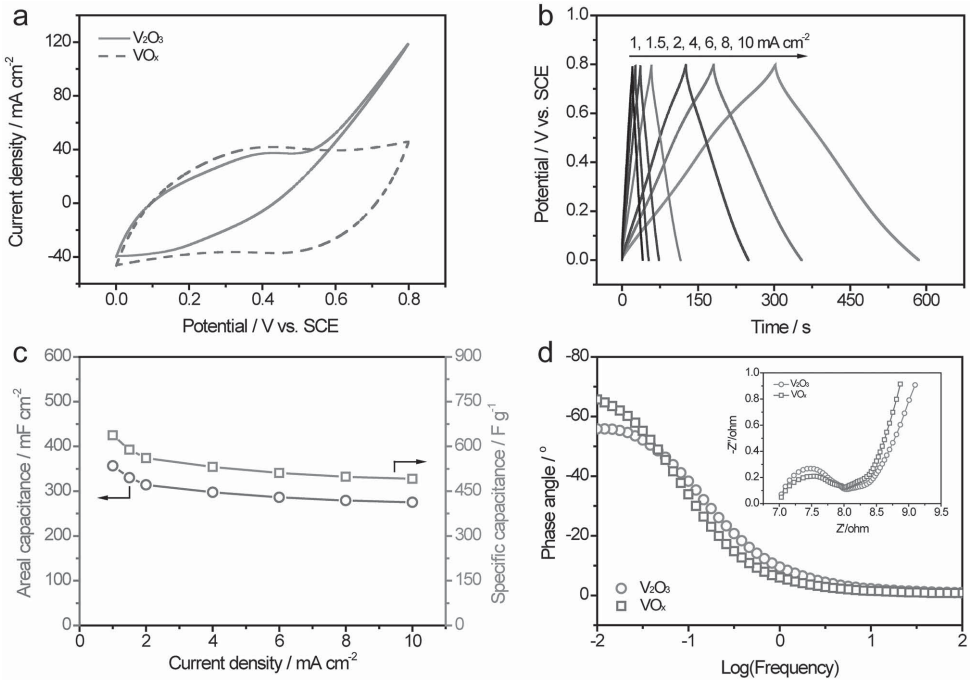

Figure 3. a) CV curves collected at 100 mV s^{-1} of V_2O_3 and VO_x electrodes. b) Galvanostatic charge–discharge curves collected at different current densities for VO_x electrode. c) Areal capacitance and gravimetric capacitance as a function of the current density for VO_x electrode. d) Bode plots and Nyquist plots collected for V_2O_3 and VO_x electrodes.

Information) into account. Then, the systematic study for VO_x electrode with oxidation time of 20 s was conducted. For comparison, the CV curve of VO_x and V_2O_3 electrodes at 100 mV s^{-1} is collected in **Figure 3**a. A steep slope appears from about 0.5 V, which reflects a violent oxidation reaction occurred at V_2O_3 electrode, and suggests that the V_2O_3 electrode can hardly fulfill the efficient charge–discharge demands of SCs at this potential range. Meanwhile, the CV profile of VO_x electrode is extremely symmetric and nearly rectangular in shape, revealing its superior charge storage ability and high efficiency. Thereby, our proposed electrochemical oxidation method could efficiently enable VO_x electrode a superior electrochemical performance. Additionally, Figure 3b depicts the charge–discharge behavior of our VO_x electrode at various current densities. The nearly isosceles triangle shape of all charge–discharge curves further confirms its excellent reversibility, high Coulombic efficiency, and good charge propagation. What is more, the calculated specific capacitances based on the electrode area and active material mass are summarized in Figure 3c, which have already excluded the contribution of the carbon cloth (Figure S4, Supporting Information). At the current density of 1 mA cm^{-2}, a highest areal capacitance of 356.8 mF cm^{-2} was calculated for the as-prepared VO_x electrode, while a corresponding gravimetric capacitance of 637.1 F g^{-1}. These values are substantially higher than most of vanadium oxides based electrodes (Table S1, Supporting Information).[3] It is also worthy to point out that a high areal capacitance of 275.2 mF cm^{-2} (corresponding gravimetric capacitance of 491.5 F g^{-1}) was maintained when the current density reached 10 mA cm^{-2}, which means a remarkable capacitance retention of 77.1%. For comparison, the similar electrodes with single valence (+4 and +5) were also prepared. (Details can be seen in Supporting Information and Figure S5.) As shown in Figure S6 (Supporting Information), the electrodes with single higher state (+4 or +5) exhibited poor performances as supercapacitor electrodes when compared to our VO_x electrode. Furthermore, inspection of Figure 3d reveals the tiny change for kinetic features of ion diffusion in the electrodes. Nyquist plots obtained for VO_x electrode show a more steeper straight line in a low-frequency region than that of V_2O_3 electrode (inset of Figure 3d), suggesting a faster ion diffusion within VO_x electrode. Additionally, the property more close to ideal capacitors was also confirmed for VO_x electrode by its higher phase angle at a low frequency of 0.01 Hz.

2.4. Cyclic Performance of VO_x Electrode

As mentioned before, cycling stability is the main obstacle for vanadium oxides materials, severely limiting their practical use in SCs. Aimed at this, we elaborately examined the long-term durability of our as-prepared VO_x electrode at a scan rate of 100 mV s^{-1} for 100 000 cycles. **Figure 4**a illustrates the correlation between the capacitance retention and performed cycles. Notably, the capacitance of VO_x electrode continuously increased in the initial cycles, which can be attributed to the active process of the electrode. In this process, electrolyte soaked into the electrode surface completely, which favored the electrochemical intercalation/deintercalation of ions, and the redox reaction on the entire surface became easier. Until 26 000 cycles, the capacitance of VO_x electrode reached the maximum value, 170.5% of its initial capacitance. After 100 000 cycles, more than 101.5% capacitance was still remained. The capacitance decrease in the

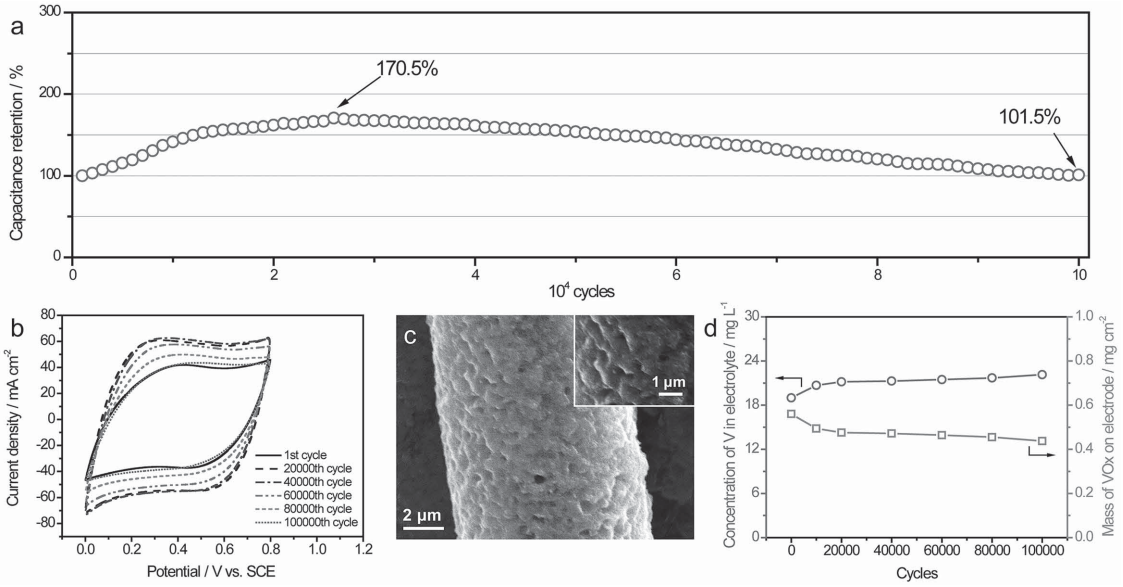

Figure 4. a) Cycling performance of VO_x electrode collected at 100 mV s^{-1}. b) CV curves collected at 100 mV s^{-1} of VO_x electrode after different cycles. c) SEM images of VO_x electrode after 100 000 cycles. d) The concentration of V element in the electrolyte and the mass loading of active materials remained in electrode after different cycles.

last 74 000 cycles might be due to the slight structural degradation induced by repeated ion intercalation/deintercalation. However, notably is that the capacitance decrease rate of our VO_x electrode is substantially slower than other reported VO_x electrodes. To our knowledge, the presented stability was the best one reported for vanadium oxides to date (Table S1, Supporting Information).[3] The corresponding CV curves of different cycles are provided, as shown in Figure 4b. As can be observed, all the CV curves show extremely symmetric and nearly rectangular shape, suggesting that the superior charge storage ability of VO_x electrode was well maintained after long cycles test. SEM study on VO_x electrode after the cycling test was performed (Figure 4c). Despite traces of further dissolution were observed, the remained active materials still kept the porous network morphology, which is almost the same as initial VO_x. In addition, we also measured the concentration of V element in the electrolyte and calculated the mass loading of active materials remained after different cycles (Figure 4d). As expected, it had a relatively fast increase of the V element concentration in electrolyte, which is consistent with the active process occurred during the cycling test. Simultaneously, the mass loading of active material had an apparent drop to 0.48 mg cm^{-2} after 20 000 cycles. During the following 80 000 cycles, the variation rate of both V element concentration in electrolyte and mass loading of active materials became slow. Hence, it is reasonably speculated that a proper proportion was reached for V^{3+}, V^{4+}, and V^{5+} after the active process, resulting in reversible conversion between them during the charge–discharge processes. Additionally, a dynamic balance may be also realized between the dissolved V in electrolyte with the active material in electrode, which will efficiently limit the further dissolve of active material in electrode.

For better understanding, additional XPS measurements were conducted to VO_x electrode after 20 000 cycles (denoted as VO_x-L1) and 100 000 cycles (denoted as VO_x-L2), as shown in Figure S7 (Supporting Information). **Figure 5**a illustrates the distribution of V with different valence states in different VO_x

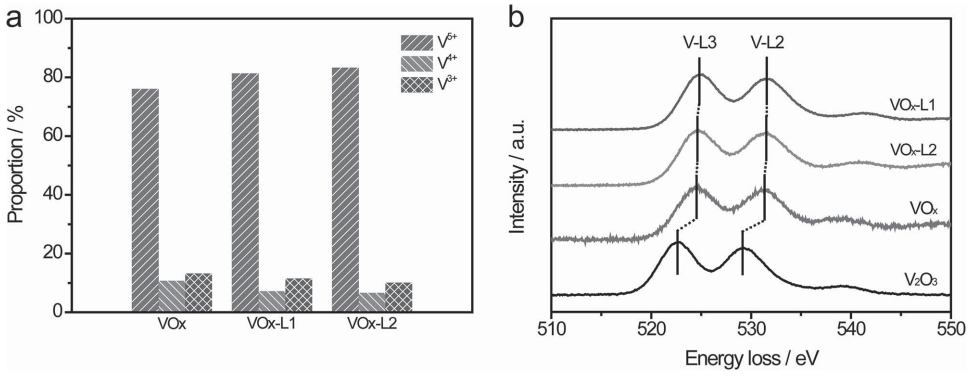

Figure 5. a) The proportion distribution of V^{3+}, V^{4+}, and V^{5+} in surface VO_x electrode after 0, 20 000 (denoted as VO_x-L1) and 100 000 (denoted as VO_x-L2) cycles. b) EELS spectra collected for as-prepared V_2O_3, VO_x, VO_x-L1, and VO_x-L2 samples.

samples. After first 20 000 cycles, the relative proportion of V^{5+} increased to 81.3%, while the relative proportion of V^{3+} and V^{4+} decreased to 11.5 and 7.2%, respectively. However, only tiny variation was observed between VO_x-L1 and VO_x-L2. Electron energy loss spectroscopy (EELS) spectra were also collected for VO_x-L1 and VO_x-L2 samples (Figure 5b). As expected, there is only tiny right-shift position of the L_2 and L_3 peak maximum for VO_x-L1 and VO_x-L2 samples, indicating the slight adjustment of V valence state for the internal samples after long-term charge–discharge processes. All these results are fully in line with our speculation.

3. Conclusion

In summary, a novel method was developed to achieve long cycling performance for vanadium oxides based SCs electrodes by tuning the valence state of vanadium. The elaborately designed experiment was realized through electrochemical oxidation of V_2O_3 with a low voltage of only 0.7 V. After the facile oxidation process, a porous film of VO_x film with amorphous structure was attained, which contains V^{3+}, V^{4+}, and V^{5+} inside the electrode. Our as-fabricated VO_x electrode exhibited a remarkable areal capacitance of 356.8 mF cm^{-2} (corresponding gravimetric capacitance of 637.1 F g^{-1}) at 0.5 mA cm^{-2}, and excellent capacitance retention of 77.1% with the current density increasing 20-fold. Most importantly, VO_x electrode exhibited an abnormal long-term cycling stability without any decay of capacitance after 100 000 cycles. The long durability of VO_x could be attributed to that a proper proportion was reached for V^{3+}, V^{4+}, and V^{5+} after the active process, enabling reversible conversion during the charge–discharge processes. Moreover, the already dissolved V in electrolyte also efficiently limited the further dissolve of active material in electrode. We hope this facile method with low cost and short time-consuming will push the practical application of vanadium oxides in SCs application.

4. Experimental Section

Preparation of V_2O_3 Nanorods: All reagents used were of analytical grade and used directly without any purification. Free-standing V_2O_3 nanorods were grown on carbon fabric cloth by a two-step process. Firstly, 0.52 g NH_4VO_3 was added to 64 mL distilled water and stirred into a pellucid solution under 90 °C. After the solution cooled down to room temperature, 0.67 g thiourea and 16 mL ethanol were added to solution, and followed by tuning the pH to ≈3 with concentrated HCl. 40 mL of this clear solution mixture together with the carbon fabric cloth (3 cm × 5 cm) was transferred to a Teflon-lined stainless-steel autoclave (50 mL volume). The sealed autoclave was heated in an electric oven at 160 °C for 6 h, and then allowed it cool down slowly at room temperature. The sample was thoroughly washed with DI water and dried. Finally, the V_2O_3 nanorods were obtained by annealing in H_2 at 600 °C for 1 h.

Preparation of VO_x Sample: A piece of V_2O_3 (0.5 cm × 2 cm) was oxidized using an electrochemical method in a conventional three-electrode cell. A Pt wire was used as a counter electrode, while a saturated calomel electrode (SCE) was used as a reference electrode. The facile electro-oxidation process was conducted using a constant voltage of 0.7 V in 5 M LiCl aqueous electrolyte for 20 s.

Materials Characterization and Electrochemical Measurements: The microstructures and compositions of electrode materials were analyzed by field-emission SEM (FE-SEM, JSM-6330F), transmission electron microscopy (TEM, FEI Tecnai G^2 F30), X-ray diffractometer (XRD, D8 ADVANCE), Raman spectroscopy (Renishaw inVia), and XPS (XPS, ESCALab250, Thermo VG). EPR tests were carried out in the X-band (9.45 GHz) with 3.20 G modulation amplitude and a magnetic field modulation of 100 kHz using a Bruker, A300-10-12 Bruker EPR spectrometer at 100 K. Cyclic voltammetry (CV), galvanostatic charge–discharge measurements, and electrochemical impedance spectroscopy (EIS) were conducted employing an electrochemical workstation (CHI 760D). The electrochemical studies of the individual electrode were directly performed after the oxidation process in a conventional three-electrode cell, with a Pt counter electrode, a saturated calomel reference electrode (SCE), and 5 M LiCl electrolyte.

Supporting Information

Supporting Information is available from the Wiley Online Library or from the author.

Acknowledgements

M.Y. and Y.Z. contributed equally to this work. The authors acknowledge the National Science Foundation of China (51472187, 51272200, 6127413, 21403306), Guangdong Natural Science Foundation for Distinguished Young Scholar (2014A030306048), and Program for New Century Excellent Talents in University (NCET-12-0911) for financial support.

Received: April 3, 2015
Published online: May 5, 2015

[1] a) Z. Yu, J. Thomas, *Adv. Mater.* **2014**, *26*, 4279; b) J. Xiao, L. Wan, S. Yang, F. Xiao, S. Wang, *Nano Lett.* **2014**, *14*, 831; c) J. Jiang, Y. Li, J. Liu, X. Huang, C. Yuan, X. W. Lou, *Adv. Mater.* **2012**, *24*, 5166; d) X. Xia, D. Chao, Z. Fan, C. Guan, X. Cao, H. Zhang, H. J. Fan, *Nano Lett.* **2014**, *14*, 1651; e) M. Yu, Y. Zhang, Y. Zeng, M. S. Balogun, K. Mai, Z. Zhang, X. Lu, Y. Tong, *Adv. Mater.* **2014**, *26*, 4724; f) X. Wu, L. Jiang, C. Long, T. Wei, Z. Fan, *Adv. Funct. Mater.* **2015**, *25*, 1648.

[2] a) M. Yu, W. Wang, C. Li, T. Zhai, X. Lu, Y. Tong, *NPG Asia Mater.* **2014**, *6*, e129; b) M. Yu, Y. Huang, C. Li, Y. Zeng, W. Wang, Y. Li, P. Fang, X. Lu, Y. Tong, *Adv. Funct. Mater.* **2015**, *25*, 324; c) C. Zhou, Y. Zhang, Y. Li, J. Liu, *Nano Lett.* **2013**, *13*, 2078; d) C. Guan, Z. Zeng, X. Li, X. Cao, Y. Fan, X. Xia, G. Pan, H. Zhang, H. J. Fan, *Small* **2014**, *10*, 300; e) C. Peng, Z. Wen, Y. Qin, L. Schmidt-Mende, C. Li, S. Yang, D. Shi, J. Yang, *Chem. Sus. Chem.* **2014**, *7*, 777; f) Z. Yu, B. Duong, D. Abbitt, J. Thomas, *Adv. Mater.* **2013**, *25*, 3302; g) G. Xu, B. Ding, P. Nie, L. Shen, J. Wang, X. Zhang, *Chem. Eur. J.* **2013**, *19*, 12306; h) F. Zhang, C. Yuan, J. Zhu, J. Wang, X. Zhang, X. W. D. Lou, *Adv. Funct. Mater.* **2013**, *23*, 3909; i) Y. Xiao, S. Liu, F. Li, A. Zhang, J. Zhao, S. Fang, D. Jia, *Adv. Funct. Mater.* **2012**, *22*, 4052; j) Z. Fan, J. Yan, T. Wei, L. Zhi, G. Ning, T. Li, F. Wei, *Adv. Funct. Mater.* **2011**, *21*, 2366.

[3] a) Z. Chen, V. Augustyn, J. Wen, Y. Zhang, M. Shen, B. Dunn, Y. Lu, *Adv. Mater.* **2011**, *23*, 791; b) J.-M. Li, K.-H. Chang, C.-C. Hu, *Electrochem. Commun.* **2010**, *12*, 1800; c) M. Li, G. Sun, P. Yin, C. Ruan, K. Ai, *ACS Appl. Mater. Interfaces* **2013**, *5*, 11462; d) S. D. Perera, B. Patel, N. Nijem, K. Roodenko, O. Seitz, J. P. Ferraris, Y. J. Chabal, K. J. Balkus, *Adv. Energy Mater.* **2011**, *1*, 936; e) X. Rui, Z. Lu, Z. Yin, D. H. Sim, N. Xiao, T. M. Lim, H. H. Hng, H. Zhang, Q. Yan, *Small* **2013**, *9*, 716; f) J. Zhu, L. Cao, Y. Wu, Y. Gong, Z. Liu, H. E. Hoster, Y. Zhang, S. Zhang, S. Yang, Q. Yan, P. M. Ajayan, R. Vajtai, *Nano*

Lett. **2013**, *13*, 5408; g) W. C. Fang, *J. Phys. Chem. C* **2008**, *112*, 11552; h) J. Shao, X. Li, Q. Qu, H. Zheng, *J. Power Sources* **2012**, *219*, 253; i) Y. Yang, D. Kim, M. Yang, P. Schmuki, *Chem. Commun.* **2011**, *47*, 7746; j) G. Wang, X. Lu, Y. Ling, T. Zhai, H. Wang, Y. Tong, Y. Li, *ACS Nano* **2012**, *6*, 10296; k) X. Pan, G. Ren, M. N. F. Hoque, S. Bayne, K. Zhu, Z. Fan, *Adv. Mater. Interfaces* **2014**, *1*, 1400398; l) H.-Y. Li, K. Jiao, L. Wang, C. Wei, X. Li, B. Xie, *J. Mater. Chem. A* **2014**, *2*, 18806.

[4] D. M. Yu, S. T. Zhang, D. W. Liu, X. Y. Zhou, S. H. Xie, Q. F. Zhang, Y. Y. Liu, G. Z. Cao, *J. Mater. Chem.* **2010**, *20*, 10841.

[5] S.-H. Lee, H. M. Cheong, P. Liu, C. E. Tracy, *Electrochem. Solid State* **2003**, *6*, A102.

[6] a) C. Wu, F. Feng, Y. Xie, *Chem. Soc. Rev.* **2013**, *42*, 5157; b) T. Zhai, X. Lu, Y. Ling, M. Yu, G. Wang, T. Liu, C. Liang, Y. Tong, Y. Li, *Adv. Mater.* **2014**, *26*, 5869.

[7] a) N. Ding, X. Feng, S. Liu, J. Xu, X. Fang, I. Lieberwirth, C. Chen, *Electrochem. Commun.* **2009**, *11*, 538; b) H. Tan, J. Verbeeck, A. Abakumov, G. Van Tendeloo, *Ultramicroscopy* **2012**, *116*, 24.

[8] a) M. Che, B. Canosa, A. Gonzalez-Elipe, *J. Phys. Chem.* **1986**, *90*, 618; b) G. Pozarnsky, A. McCormick, *Chem. Mater.* **1994**, *6*, 380.

[9] a) T. D. Manning, I. P. Parkin, R. J. H. Clark, D. Sheel, M. E. Pemble, D. Vernadou, *J. Mater. Chem.* **2002**, *12*, 2936; b) C. Piccirillo, R. Binions, I. P. Parkin, *Chem. Vap. Deposition* **2007**, *13*, 145.

[10] M. Demeter, M. Neumann, W. Reichelt, *Surf. Sci.* **2000**, *454*, 41.